Using a Reanalysis-Driven Land Surface Model for Initialization of a Numerical Weather Prediction System

ÅSMUND BAKKETUN,[a,b] JOSTEIN BLYVERKET,[a] AND MALTE MÜLLER[a,b]

[a] *Development Centre for Weather Forecasting, Norwegian Meteorological Institute, Oslo, Norway*
[b] *Department of Geosciences, University of Oslo, Oslo, Norway*

(Manuscript received 28 October 2022, in final form 8 August 2023, accepted 16 August 2023)

ABSTRACT: Realistic initialization of the land surface is important to produce accurate NWP forecasts. Therefore, making use of available observations is essential when estimating the surface state. In this work, sequential land surface data assimilation of soil variables is replaced with an offline cycling method. To obtain the best possible initial state for the lower boundary of the NWP system, the land surface model is rerun between forecasts with an analyzed atmospheric forcing. We found a relative reduction of 2-m temperature root-mean-square errors and mean errors of 6% and 12%, respectively, and 4.5% and 11% for 2-m specific humidity. During a convective event, the system was able to produce useful (fractions skill score greater than the uniform forecast) forecasts [above 30 mm $(12\ \text{h})^{-1}$] down to a 100-km length scale where the reference failed to do so below 200 km. The different precipitation forcing caused differences in soil moisture fields that persisted for several weeks and consequently impacted the surface fluxes of heat and moisture and the forecasts of screen level parameters. The experiments also indicate diurnal- and weather-dependent variations of the forecast errors that give valuable insight on the role of initial land surface conditions and the land–atmosphere interactions in southern Scandinavia.

KEYWORDS: Numerical weather prediction/forecasting; Short-range prediction; Data assimilation; Land surface model; Model initialization

1. Introduction

The land surface interacts with the atmosphere by exchanging mass and energy. Incoming solar radiation is partitioned into longwave radiation, latent, sensible, and ground heat flux. Precipitation is distributed into runoff, drainage, and evapotranspiration. The distribution between the different responses depends on the atmospheric state and the condition of the land surface. Due to the capacity of the soil to store heat and water, the land surface has a memory of past weather. Therefore, anomalies can sustain beyond the synoptic time scale and have an impact on the following evolution of the atmosphere (Seneviratne et al. 2013). Soil moisture (SM) is particularly important for the distribution of available energy into latent and sensible heat, and while a general relationship between SM and precipitation is not established, it is evident that SM can influence the triggering, timing, positioning, and amount of precipitation, particularly in conditions with weak synoptic-scale forcing (Findell and Eltahir 2003; Koster et al. 2006; Barthlott and Kalthoff 2011; Cioni and Hohenegger 2017; Henneberg et al. 2018; Baur et al. 2018).

In numerical weather prediction (NWP) and climate models, the lower boundary is represented by physically based schemes in a land surface model (LSM), which solves the moisture and energy budgets given the atmospheric conditions (Noilhan and Mahfouf 1996; Decharme et al. 2011; Balsamo et al. 2009; Best et al. 2011; Lawrence et al. 2019; Fisher and Koven 2020). The LSMs are driven by atmospheric forcing (temperature, humidity, precipitation, wind, pressure, and radiation) and use this input to calculate the fluxes required by the atmosphere at the lower boundary (latent and sensible heat, longwave radiation, momentum, and moisture flux).

The forecast errors of the land surface can be separated into model errors, errors in forcing data, and errors of representativeness. The latter is due to model resolution and auxiliary datasets. Model errors involve simplification or missing formulation of real processes, and should ideally be reduced through the development of physical parameterization or optimization of model parameters. Last, errors in the forcing data are the motivation for performing land data assimilation (LDA). Maggioni et al. (2012) found that a combination of forcing and model uncertainty produces the best estimate of the SM forecast uncertainty compared to each of them individually.

For NWP, realistic initialization of the land surface is important to produce accurate short and medium range forecasts (de Rosnay et al. 2014). An objective approach to achieve realistic initial conditions is through data assimilation (DA), where observations and model data are combined in an optimal way given their respective uncertainties. In NWP and LDA systems, surface sensitive observations like 2-m air temperature, relative humidity (Mahfouf et al. 2009), and snow depth (de Rosnay et al. 2014) are used to update the surface state variables. Several systems also use satellite-derived surface SM in their land surface analysis (de Rosnay et al. 2014; Albergel et al. 2017; Blyverket et al. 2019; Draper and Reichle 2019; Gómez et al. 2020; Seo et al. 2021). In LDA systems, the observations are embedded into the model using sequential DA schemes including optimal interpolation (OI), which uses empirical relationships between

Denotes content that is immediately available upon publication as open access.

Corresponding author: Åsmund Bakketun, asmundb@met.no

DOI: 10.1175/WAF-D-22-0184.1

the soil state variables and observations (Mahfouf 1991); the extended Kalman filter (EKF), which computes the linearized observation operator from perturbed simulations (Mahfouf et al. 2009; Draper et al. 2009; Albergel et al. 2017); or the ensemble Kalman filter (EnKF) using ensemble information to represent the background error covariance matrix (Reichle et al. 2002; Ghent et al. 2010; Draper et al. 2012; Blyverket et al. 2019; Seo et al. 2021). The two latter schemes are able to account for "uncertainty of the day," but are computationally more expensive as they require ensembles of the surface model.

Initialization approaches using land surface reanalysis products as initial conditions have also been studied in the literature, e.g., Santanello et al. (2019) studied the impact of SM uncertainty on precipitation forecasts over the continental United States. They used available "off the shelf" products, and satellite data directly as initial fields and found an impact on the ambient weather verification statistics. However, they emphasize that forecast validation scores can be improved for the wrong reasons, and understanding the affected process chains is crucial when introducing new input data. Reichle et al. (2017) showed how model precipitation corrected using observations as input for the land surface simulations in a global reanalysis gave improvements in surface fluxes and 2-m temperatures. Koukoula et al. (2021) carried out numerical simulations with different SM and surface temperature (ST) initialization over the same region during a cold and a warm season. They found no consistent improvement of precipitation forecasts with more realistic surface state, but an enhanced spatial skill of precipitation forecasts during the warm period where precipitation events are dominated by convection.

In the literature, Scandinavia is often found to have weak land–atmosphere coupling strength (e.g., Koster et al. 2006; van den Hurk et al. 2012), and receives small increments or impact from LDA systems (e.g., de Rosnay et al. 2014; Draper and Reichle 2019). However, the time scale and model resolution can influence these results. Local high-resolution studies are thus needed to better understand the role of the land surface in this region. The utilization of satellite observations is also challenging over high latitudes and complex terrain (Wrona et al. 2017). Thus, optimal use of the existing observation networks is important for realistic initialization of the land surface.

In this study we assess the following questions: 1) Are NWP forecasts over the Nordic countries sensitive to the land surface initial condition, in particular during convective precipitation? 2) Can we, by correcting forcing data for the LSM with screen level observations, improve the surface analysis relative to a sequential DA method and potentially reduce the forecast errors?

A description of the model system used for the numerical simulations, initialization strategies, and validation metrics is given in section 2. The experiment results and analysis are presented in section 3, a summary and discussion follow in section 4, and the conclusion is given in section 5.

2. Model description and experimental design

a. Model description

In this study, numerical simulations are performed using the Harmonie-AROME NWP system. The Harmonie-AROME model system is used for research and operational weather forecasting in several European countries including the Meteorological Co-operation on Operational NWP (MetCoOp) (Müller et al. 2017). The model core is the convective permitting, nonhydrostatic Applications of Research to Operations at Mesoscale (AROME) model (Seity et al. 2011).

The lower boundary is treated by the externalized surface (SURFEX) model (Masson et al. 2013). SURFEX handles sea, inland water, urban area, and land in four individual tiles per grid cell. The land tile is represented by the Interactions between Soil, Biosphere, and Atmosphere (ISBA) LSM (Noilhan and Mahfouf 1996; Calvet et al. 1998; Decharme et al. 2011). In this study, the diffusion version of ISBA is used, where the soil column is discretized into 14 layers with the lowermost boundary at 12 m below the surface. Heat transfer is modeled with the Fourier diffusion equation and water interception by Darcy's law for porous media (Decharme et al. 2011). The land tile is split into two patches representing open land and forest. The two patches have separate soil columns with moisture and energy budgets. Over the forest patch, we activate the explicit canopy scheme, the multienergy balance (MEB) option (Boone et al. 2017; Napoly et al. 2017).

Bare soil evaporation is active in the 0.01-m top layer, while transpiration removes SM from soil layers in the root zone, whose thickness depends on the vegetation type. The transpiration rate is limited by SM stress, which is proportional to the relative SM between the wilting point and field capacity.

In the present study, the 43h2.1 model version of the Harmonie-AROME system is set up on a domain covering the southern part of Norway, consisting of 250 × 250 grid cells with a horizontal resolution of 2500 m. The domain was selected to cover a convective precipitation event and at the same time keep the computational cost low. The domain also covers the relatively homogeneous areas in Norway east of the mountain ridge, where thunderstorms are most likely caused by land–atmosphere interactions. Orography and soil texture datasets are taken from GMTED2010 (Danielson and Gesch 2011) and SOILGRID (Hengl et al. 2017), respectively. SURFEX reads vegetation and cover types from the ECOCLIMAP dataset (Masson et al. 2003; Faroux et al. 2013). In our experiments the recent ECOCLIMAP second generation is used, which is based on the "European Space Agency–Climate Change Initiative" (ESA-CCI) land cover map v1.6.1 (https://www.esa-landcover-cci.org/?q=node/158 accessed 28 September 2022).

b. Boundaries

At the lateral boundaries, we use model fields from the operational Integrated Forecast System (IFS)-high-resolution (HRES) cy46r1 provided by the European Centre for Medium-Range Weather Forecasts (ECMWF). IFS-HRES has a horizontal resolution of 9 km with hourly output. In IFS the land surface is treated by the Tiled ECMWF Scheme for Surface Exchanges

over Land (TESSEL) (Balsamo et al. 2009) and has a similar treatment of heat and moisture transfer in the soil as ISBA. A vertical interpolation of prognostic soil variables from the TESSEL to the SURFEX grid is performed in the first initialization of the system.

c. *The Nordic Analysis*

The Nordic Analysis product is produced by MET Norway and covers Scandinavia with a spatial resolution of 1 km. The product is published hourly, about 15 min after the reference time. The dataset contains surface parameters including 2-m temperature and precipitation. The analysis background is obtained from the latest available MetCoOp EPS (MEPS) forecast. The precipitation forecast is corrected using observations from MET Norway's radar network and station based rain gauges, described in Lussana et al. (2021). The 2-m temperature forecast is downscaled and corrected using high-resolution elevation data and temperature observations from synoptic weather stations and citizen-owned instruments. The dense citizen station network undergoes a spatial quality control prior to entering the analysis. See Nipen et al. (2020), Båserud et al. (2020), Lussana et al. (2019) for a detailed description of the quality control and analysis method and https://github.com/metno/NWPdocs/wiki/MET-Nordic-dataset for a description of the product.

d. *Experimental design*

The model system is set up with two different initialization strategies, described below, during July 2019 over southern Norway (Fig. 1). Both experiments are cold started from IFS-TESSEL model fields on 0000 UTC 1 July 2019 and use 3-h cycling throughout the experiment. The simulations are allowed to adapt to the vertical grid of SURFEX and the high-resolution atmospheric forcing over a 12-day period. Forecast verification is then performed on the remaining 19 days of July.

1) REFERENCE SIMULATION

A reference simulation, hereafter REF, is set up similar to an operational NWP system. LDA is performed every 3 h using 2-m temperature and relative humidity to update SM and ST. The station observations are horizontally interpolated using an OI (Mahfouf 1991). The 2D observation fields are then assimilated vertically into the soil with a SEKF (Albergel et al. 2017). The upper air is updated using the 3D-Var scheme as described in Müller et al. (2017) and references therein. The surface and atmosphere interact during the forecast integration, then, their 3-h forecast is used as the background state in the next DA cycle, see Fig. 2a.

2) OFFLINE CYCLING

An alternative initialization strategy (OFL) is applied in a parallel experiment. Between each 3-h forecast cycle, the surface model is run offline with analyzed atmospheric forcing. The 2-m temperature and precipitation data are obtained from the hourly Nordic Analysis product described in section 2c. Other parameters required for the atmospheric forcing are taken from the MEPS forecasts directly. The forcing preparation interpolates data from the Nordic Analysis and MEPS onto the experiment domain. SURFEX interpolates the input forcing linearly in time between the full hours.

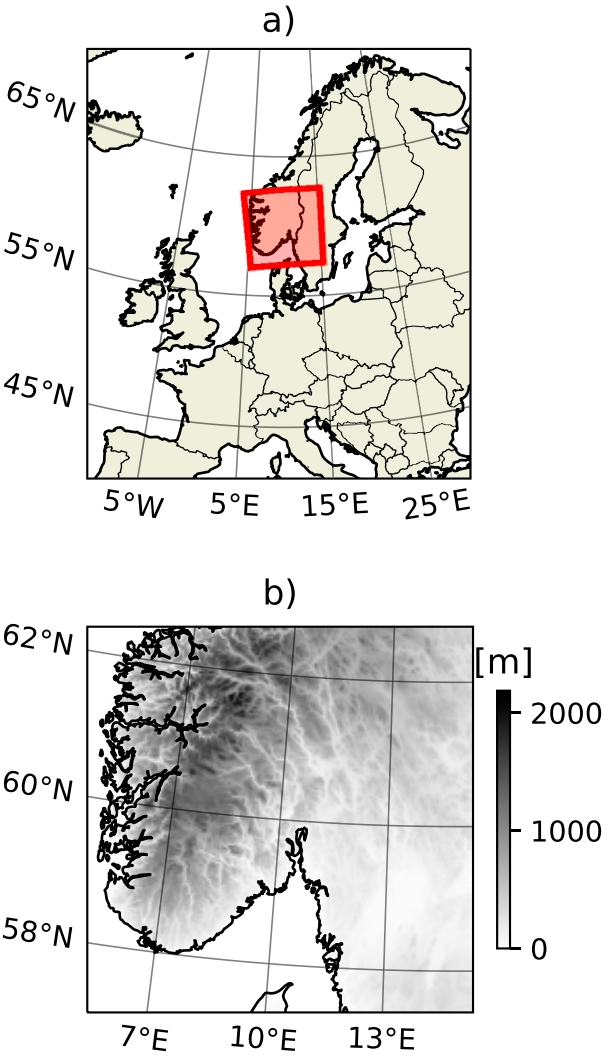

FIG. 1. (a) Location of domain and (b) model domain with elevation in shading.

The coupled forecasts are initialized every 3 h where the initial surface state is taken from the end of the offline run. The upper air is updated in a similar manner as in REF. The initial surface condition for each forecast cycle is unaffected by the previous coupled simulation, contrary to the atmosphere which can be influenced over time by the surface. The two initialization strategies are presented in Fig. 2.

We considered following the method proposed by Fairbairn et al. (2019) and use the same atmospheric analysis for REF and OFL. In addition to reducing the computational cost, the impact of the surface initialization is isolated for each forecast. However, it was decided to keep the atmospheric loop intact and let the surface influence the upper-air state throughout

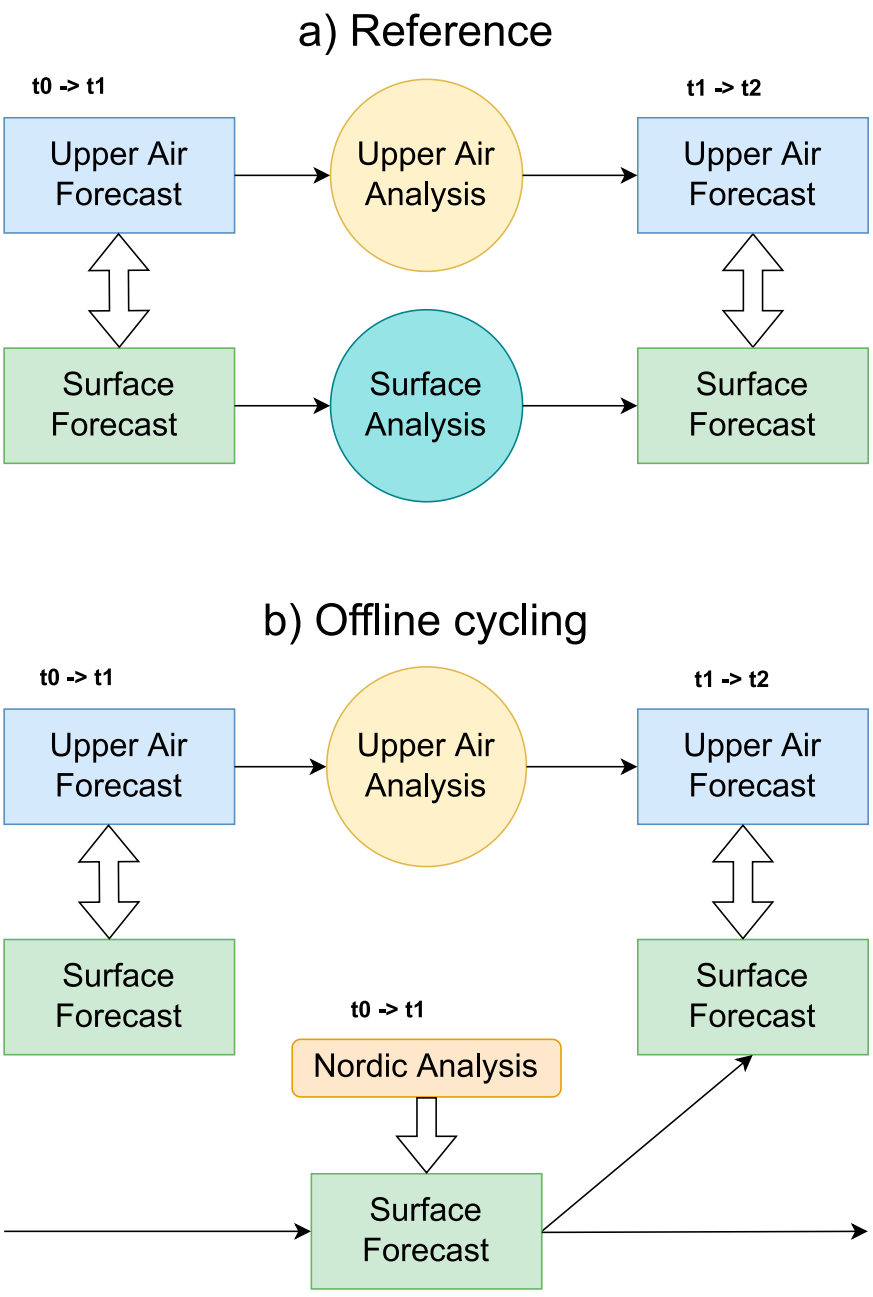

FIG. 2. Schematics of (a) the reference and (b) offline cycling steps. Arrows indicate the direction of information flow.

the experiment period. They found that the short term sensitivity to land surface initialization was reduced when using external atmospheric analyses, which would be undesirable in our study of short range forecasts.

e. Validation data

Validation of screen level variables is based on synoptic weather stations available from the frost API maintained by the Norwegian Meteorological Institute (https://frost.met.no/index.html, visited on 11 October 2022). The domain contains up to 161 stations measuring 2-m temperature, 2-m relative humidity, 10-m wind speed, and surface precipitation amount. For spatial validation, the Nordic Analysis precipitation product (Lussana et al. 2021) is used, after it is projected to the model grid using a nearest neighbor method. Both in situ and satellite observations were considered for validation of the modeled soil variables. A small in situ network of SM exists in Norway, and satellite products from passive L-band microwave sensors could potentially be utilized. However, their footprints of point to several tens of kilometers, respectively,

introduce large errors of representativeness over the heterogeneous land surface in the domain. We considered their uncertainty to be too large for validation of the model experiments.

f. RMSE

The root-mean-squared error (RMSE) is calculated between model (f) and observation (o) as

$$\mathrm{RMSE}_j = \sqrt{\frac{1}{n}\sum_{i=1}^{n}(f_i - o_i)^2}. \quad (1)$$

To assess the confidence interval of the RMSE, a bootstrap is performed by computing RMSE_j for $j = 1, \ldots, m$ batches where each batch consist of n random samples from all pairs drawn with replacement. $m = 1000$ was chosen and n was set equal to the total number of model–observation pairs.

g. Fractions skill score

The fractions skill score (FSS) (Roberts and Lean 2008) is used to quantify the impact of soil initial conditions on precipitation at different spatial scales. The score is computed relative to the Nordic Analysis product and compares the fraction of occurrence, for example precipitation above a certain threshold, within a neighborhood of the simulation. Typically the score increases asymptotically with increasing length scale. A perfect score of one is obtained if the fraction of occurrences is equal in the two datasets over the entire domain. In this study, fractions skill score is computed for 12-h accumulated precipitation during a selection of precipitation events.

3. Results

The mean temperature in southern Norway in July 2019 was 0.5–2 K warmer than the 1960–90 climatological mean (Grinde et al. 2019). Temperature anomalies were ranging from 0.5 K in coastal areas to 3–4 K in inland and mountainous areas. The precipitation amounts were close to normal on average in July 2019, but with significant regional anomalies. In the northeast of the domain about 50% of the climatological mean precipitation (for July) has been observed, while in the southwest part of the domain it has been about 200%. Daily precipitation from observations and the REF model simulation are shown in Fig. 3. The simulation period includes one convection event on 13 July and two events of large-scale precipitation around the dates of 21 and 30 July. While the two large-scale events are well captured at the observation locations, only small precipitation amounts are seen for the 13 July case. However, precipitation amounts above 50 mm were observed by the radar product during the event (see Fig. 9).

a. Model comparison

In the following, soil states from REF and OFL are compared at analysis times. In general, OFL is colder than REF particularly in mountainous areas north and midwest in the domain (Fig. 4a). The structure of the mean differences in the northern part of the domain aligns with the topography in the area. This is the highest

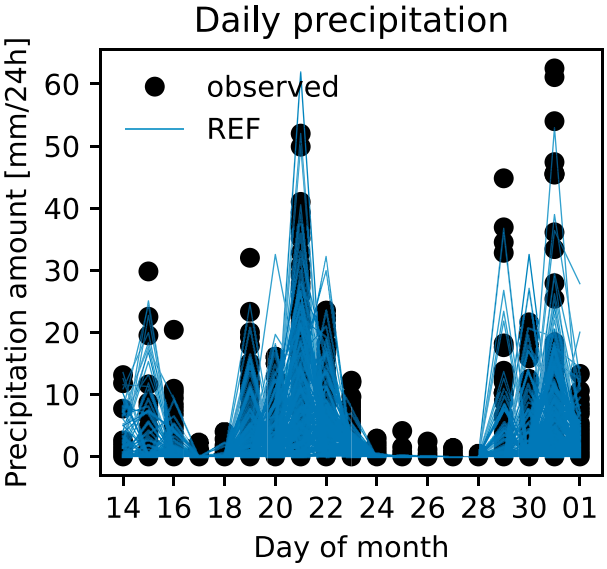

FIG. 3. The 24-h accumulated precipitation measured at 0600 UTC at all observation stations in the model domain during July 2019. Filled circles represent station observations, and blue lines represent model values at the station locations. Model values are composites of +6- to +18-h accumulated precipitation from REF initialized at 0000 and 1200 UTC during July 2019.

elevated area in Norway and has steep gradients into valleys and fjords. The Nordic Analysis is expected to provide more detailed 2-m temperature estimates in this terrain due to the higher observation density and the finer resolution of the elevation model. The coastal and inland areas in the southeastern part of the domain have less mean difference between the experiments. The ST standard deviation of REF is approximately 4.5 K averaged over the domain. The mean differences thus reach about 50% of the variation of the variable itself. On the coarser scale the negative ST differences are collocated with positive SM differences (Fig. 4b). However, the smaller-scale structures of SM differences are different from ST. The most striking difference is the relatively small-scale clusters of positive and negative differences in the eastern part of the domain. These patterns are similar to the precipitation fields from the convective case on 13 July (shown later in Fig. 9). We also note that the structures related to topography are not present for SM. In REF, SM has a domain average standard deviation of 0.05, the mean SM differences between OFL and REF thus has the same magnitude, or even higher in certain areas, than the variation of the variable itself. Mean differences of latent and sensible heat flux are consistent with the patterns of SM differences (Figs. 4c,d). Areas where OFL is wetter(drier) than REF are associated with increased(decreased) latent heat flux and decreased(increased) sensible heat flux. The results indicate that the evaporation is limited by SM during the extent of the experiments and will thus impact the forecast in the following ways: First, the modification of the surface fluxes impact near surface variables like 2-m temperature and humidity. Second, the modified fluxes cause a change in the planetary boundary layer depth between the two experiments, where an increase (decrease) in SM cause a decrease (increase) of the

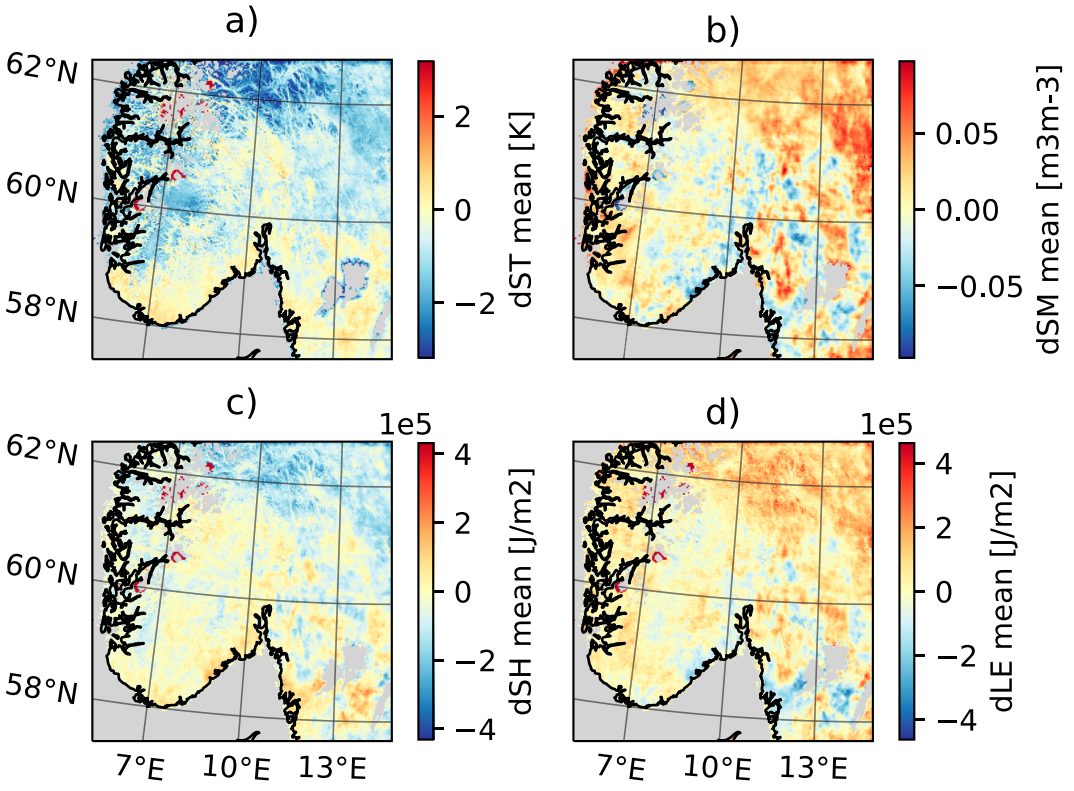

FIG. 4. Monthly mean difference between OFL and REF for (a) soil temperature and (b) soil moisture model level 2 (1–4 cm) is shown. Monthly mean difference in (c) sensible and (d) latent heat flux. Blue values indicate smaller (colder/drier) values in OFL, and red values indicate larger (warmer/wetter) values in OFL compared to REF.

boundary layer thickness (not shown). The latter impacts the formation of clouds and precipitation.

In Fig. 5, the sign of ST and SM differences agree with Fig. 4, where OFL is being primarily colder and wetter than REF. There is a diurnal signal of the ST differences (dST), with a systematic colder ST in OFL during morning hours. This bias propagates into deeper model layers over the duration of the experiment. During the night, OFL has a warmer mean temperature across the domain compared to REF. Higher SM content is seen in the upper four layers (20 cm) in OFL compared to REF. The difference is introduced during the convective case on 13 July and increased during the large-scale precipitation around 21 July. In the following 2 weeks after the precipitation event the differences gradually decline. The warmer ST of OFL during night is enhanced during this period. Around 29 July, the signal of the last precipitation event is seen in the SM difference.

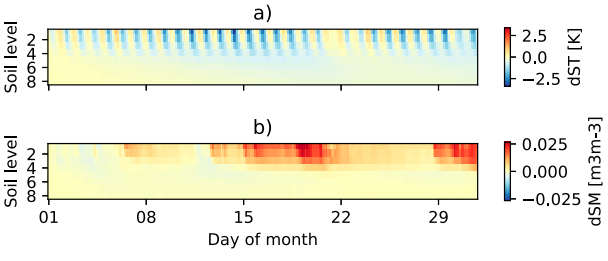

FIG. 5. (a) Domain average soil temperature and (b) SM bias vs time (July 2019) for the upper eight model soil levels (0–1 m).

b. *Validation against in situ measurements*

The validation is performed for the last 19 days of July 2019. A total of 161 stations are used in the comparison. Model minus observation pairs are computed every 3 h whenever available, and all pairs are used without additional quality control or filtering.

In terms of 2-m temperature, OFL has smaller RMSE relative to REF for all lead times, with significant difference at the 5%–95% confidence interval (Fig. 6). At initialization time, a 0.4-K difference in RMSE is found. From forecast lead times after hour 3, the difference in RMSE is reduced to about 0.1 K. Over a 48-h forecast the RMSE increased by 0.1–0.2 K. There is also a 12-h variation in both experiments with higher RMSE at lead times 3, 15, 27, 36, and 48 h. Investigation of daily variation (not shown) reveals that larger errors are found in the afternoon (maxima at 1500 UTC), and that errors are smaller during morning (minima at 0600 UTC). We also note that the distance between the RMSE of OFL and REF is larger during the local minima (morning). Over all stations and all lead times this corresponds to an RMSE reduction of 6% in OFL relative to REF.

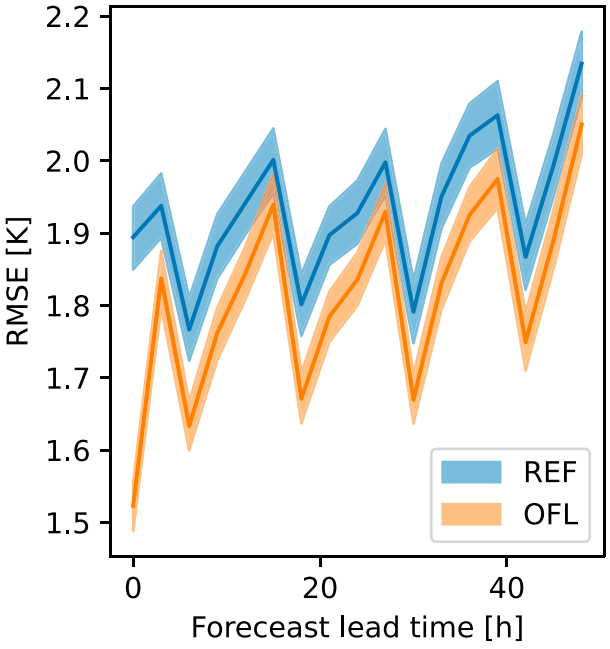

FIG. 6. RMSE of 2-m temperature forecasts with 5%–95% confidence intervals in shading obtained with bootstrap of $n = 4512$ model–observation pairs.

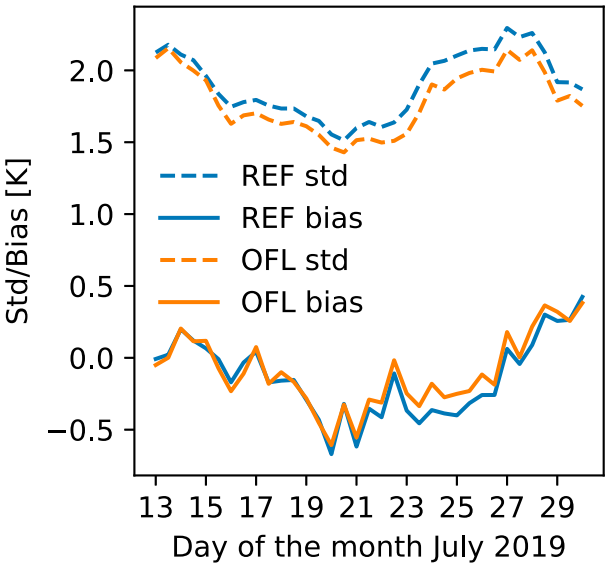

FIG. 7. The 2-m temperature errors for each 48-h forecast including every 3-h lead time, mean (solid), and standard deviation (dashed) against forecast initialization time.

Time series presented in Fig. 7 indicate that during the first three days, the experiments have relatively large standard errors. Convective-scale precipitation dominated in this period. In the following days, a large-scale low pressure system brought significant amounts of precipitation to the whole domain, and the standard errors of 2-m temperature are smaller in this period. However, a negative temperature bias is seen in both experiments. From 23 to 28 July, no precipitation fell and the 2-m temperature standard errors increased during this period. Simultaneously, OFL improves over REF in terms of mean temperature error. Eventually a new large-scale system entered the domain and the standard errors decreased. During the dry period OFL has smaller mean and standard errors for all forecasts relative to REF. Relative to REF, OFL has a reduction in mean errors of 12% and smaller mean errors at 55% of the observation sites. For specific humidity (not shown), a significant reduction in RMSE is found for the first 6 forecast hours and a consistent reduction throughout the 48 h. A similar diurnal signal as for 2-m temperature is also seen for the humidity. In terms of error standard deviation time series, OFL has smaller errors than REF for the whole simulation period except the first 2 days from 13 to 15 July. The mean errors are overall similar between the experiments except between the two large-scale precipitation events from 23 to 28 July where OFL has reduced bias. Relative to REF, OFL has a reduction of 4% in RMSE, 11% in bias with reduction in mean errors at 60% of the measuring sites. For wind speed, surface pressure and precipitation, no significant difference in summary statistics was found between OFL and REF (not shown).

Maps of the RMSE of REF and the differences in RMSE (dRMSE) between OFL and REF are shown in Fig. 8. Most stations have RMSE values between 1 and 2 K, but higher values are seen in the western mountain areas, where elevation differences between model and observation can occur, introducing systematic errors. The dRMSE Fig. 8b indicates that most stations have lower RMSE in OFL in all parts of the domain. There is a slight tendency that more stations have negative dRMSE in the northeastern part of the domain, and that fewer stations have values significantly different from zero in mountainous regions.

c. *Precipitation events*

In the following, the convective precipitation case 13 July 2019 is analyzed in more detail. This case was driven by cool air aloft combined with strong heating of the land surface which induced a sea breeze and eventually leading to individual thunderstorm cells in the afternoon. The total accumulated precipitation for the Nordic Analysis and for the REF and OFL simulations is presented in Fig. 9. The Nordic Analysis product has more intense precipitation than REF and OFL, especially in the southern part of Norway and the eastern part of the domain. In the Nordic Analysis product, the precipitation reaches further into the mountainous regions over southern Norway. The difference between REF and OFL is less pronounced, but there are deviations of the placement of showers and also differences in intensity.

To evaluate the impact of land surface initialization on the spatial characteristics of the convective precipitation event we compute the FSS for 12-h precipitation from lead time 12 to 24 (Fig. 10a). In general, the score increases as scale increases and depending on threshold, the forecasts reach the skill of a uniform forecast at scales between 75 and 150 km. Higher thresholds result in lower FSS scores. Comparing REF and OFL the figure indicates better agreement with the Nordic

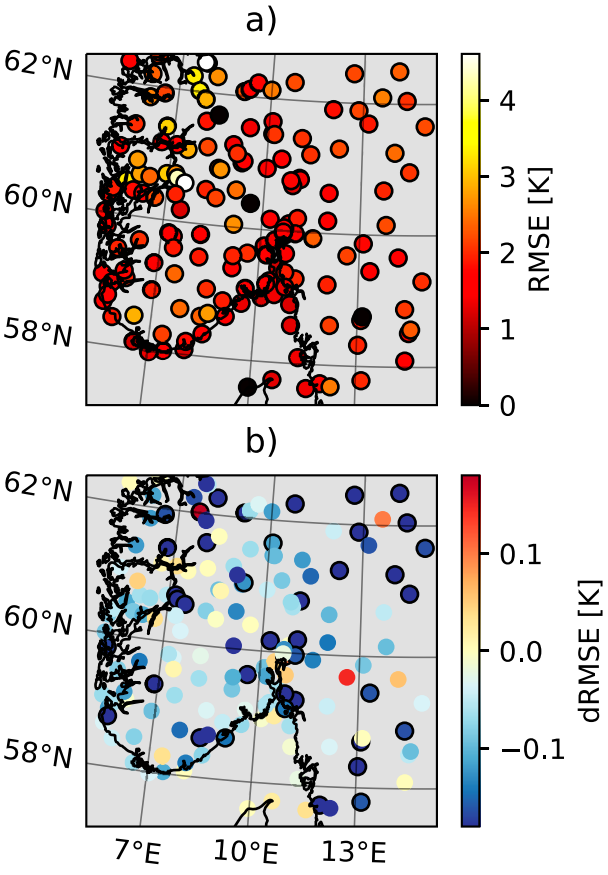

FIG. 8. (a) The 2-m temperature RMSE for REF at forecast hour 3, all forecast cycles are included. (b) Difference in RMSE between OFL and REF (dRMSE = $\mathrm{RMSE_{OFL}} - \mathrm{RMSE_{REF}}$); negative (blue) values indicate smaller RMSE of OFL relative to REF. In (b) dots with edge lines have a difference significant at the 25%–75% confidence interval.

Analysis precipitation in the OFL simulation for the higher thresholds. For a 30-mm threshold, OFL produces a useful forecast at about 100-km scale, while REF fails to reach the skill of a uniform forecast for any neighborhood size less than 200 km.

The forecast initialized at 0000 UTC 20 July 2019 had precipitation covering large parts of the domain with 12-h accumulated rain amounts over 40 mm $(12\ \mathrm{h})^{-1}$ (Fig. 11). The Nordic Analysis differs in terms of placement of the most intense precipitation from REF and OFL which are more similar. The most pronounced difference between OFL and REF is in the northeastern corner where OFL has slightly more accumulated precipitation.

Figure 10b shows FSS for the 20 July case. Values are in general higher than in the convective case, and the scale of useful forecasts lies around 25 to 50 km depending on the threshold. In this case, there is no difference between REF and OFL in terms of FSS.

The northeastern part of the domain was on average colder and wetter in OFL compared to REF (Fig. 4). While the stations with reduced 2-m temperature RMSE are located across the domain, they are slightly overrepresented in the northeastern corner (Fig. 8b). Further, Figs. 9 and 10b show larger precipitation amounts over the same area in the Nordic Analysis than modeled. This indicates that the different precipitation forcing can introduce systematic differences in soil state over a month, and further impact surface fluxes and the following validation statistics of 2-m temperature and humidity.

d. *Correlation of ΔP and ΔSM*

In the following, we analyze the spatial correlation between the difference in precipitation (Nordic Analysis − REF) during a fixed precipitation event at time t_e [$\Delta P(t_e)$] and the SM difference (OFL − REF) at times t [$\Delta\mathrm{SM}(t)$]. Note that the OFL surface is forced by the Nordic Analysis product. As a result, the SM patterns are thus consistent with the analysis product and not its own precipitation at the analysis times:

$$R(t) = \mathrm{corr}[\Delta P(t_e),\ \Delta\mathrm{SM}(t)]. \tag{2}$$

The Pearson correlation coefficient is computed over all grid points to quantify the relationship between precipitation at a single event and SM patterns before, during and after the event. For each analysis time t, we evaluate $R(t)$ for the 13 July event (t_e) and obtain a time series of correlations presented in Fig. 12.

Prior to the event on 13 July, the SM difference $\Delta\mathrm{SM}(t)$ between OFL and REF has no correlation with $\Delta P(t_e)$. During and shortly after the event the correlation is at its maximum and steadily decreases in the following days. Correlation values which are larger than the pre-event values (significant at 95% confidence level) persist until about the next event one week later and continue until the 29 July precipitation event.

The decay of correlation between $\Delta P(t_e)$ and $\Delta\mathrm{SM}(t)$ as t increases, can be interpreted as a measure of SM "memory" of the sensitivity of a precipitation event. High values indicate that the differences in precipitation are collocated with the differences in the SM fields. For the 13 July case, enhanced values were seen for a 2-week time period, indicating that the SM fields kept a memory of the precipitation event during this period (Fig. 12).

4. Discussion

Accurate description of land surface characteristics such as SM and temperature is highly relevant for operational NWP, by constraining the model to evolve closely to the real system. In the present study, we have implemented an alternative approach for land surface initialization in a convective-scale NWP model. The approach utilizes a novel product (Nordic Analysis) which is based on operational NWP forecasts, synoptic observations, crowd sourced measurements and radar precipitation. By performing a parallel offline run with the surface model from the previous initialization time to the current, driven by the Nordic Analysis product, we expect to obtain a more realistic surface initial state for the next forecast integration.

We performed a 1-month short-range reforecast experiment over southern Norway with the new method and with the reference model. The study period contains a case of

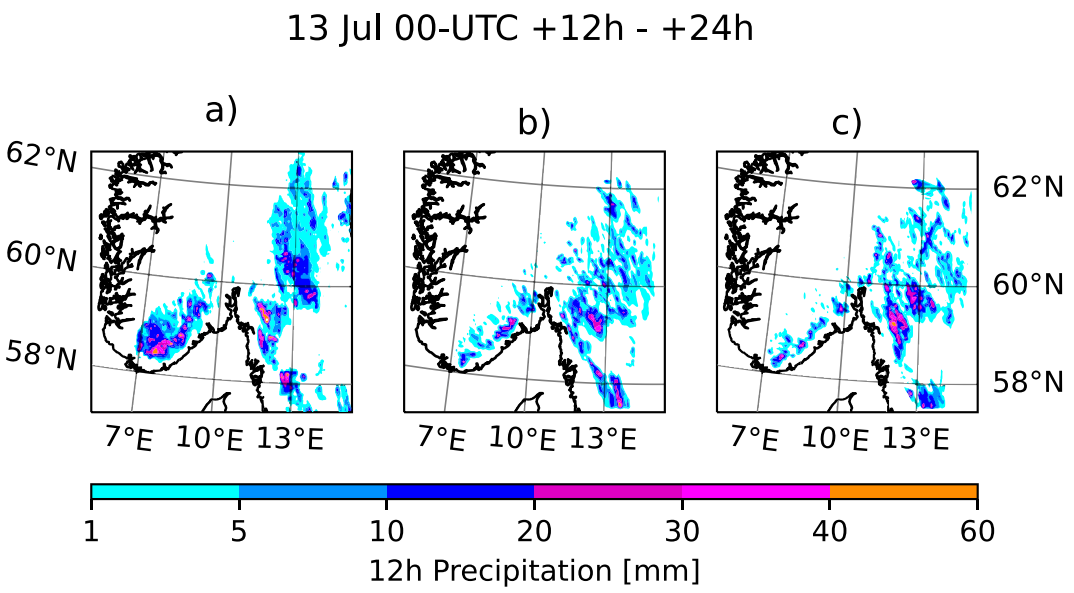

FIG. 9. The 12-h accumulated precipitation during 1200–2400 UTC 13 Jul 2019. (a) Nordic Analysis product, (b) REF, and (c) OFL.

convective precipitation and several large-scale frontal precipitation events. The two reforecast experiments are compared against each other and are validated against synoptic observations and against the Nordic Analysis product.

It is evident that the SM is sensitive to precipitation for an extended period after a precipitation event. The areas where the two experiments differ in terms of SM, coincide with large precipitation amounts during the convective case, and the spatial patterns in SM anomalies persist for several weeks. Increased SM generally causes decreased temperature due to the energy required for evaporation and thus restricting sensible heating. Our results indicate that the difference in precipitation forcing between the experiments, leading to SM anomalies, causes a change in Bowen ratio and a following shift in mean temperature in parts of the domain. SM memory and its impact on the atmosphere has been extensively studied in the literature

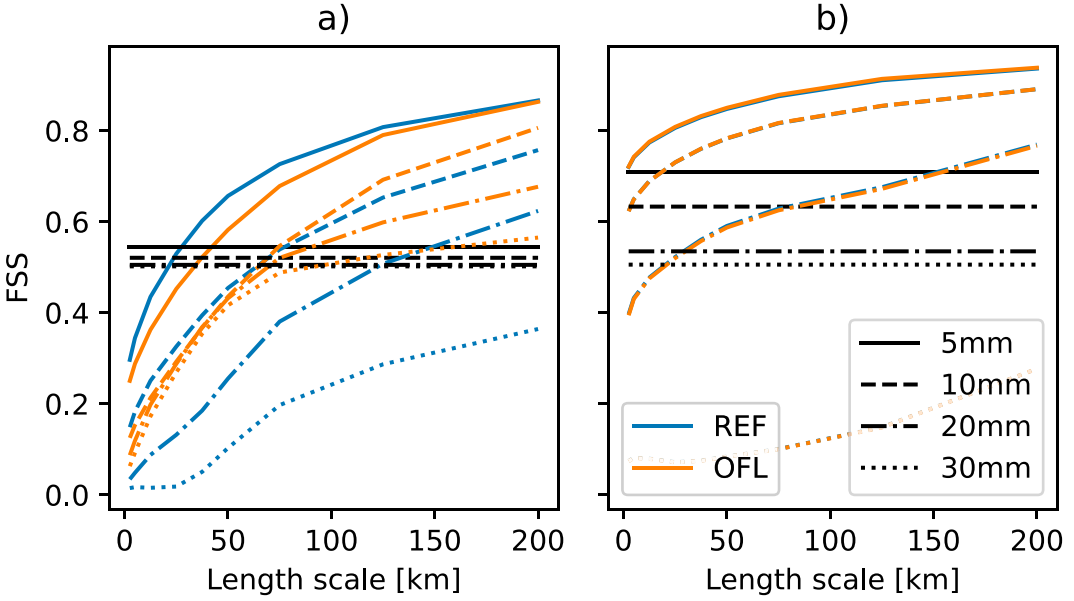

FIG. 10. FSS for 12-h precipitation from (a) 13 Jul and (b) 20 Jul 2019 relative to the Nordic Analysis precipitation product. FSS is plotted for different precipitation thresholds vs the width of the neighborhood square. The model data are accumulated precipitation from +12 to +24 h after initialization (0000 UTC). Black lines indicate the uniform skill that is considered a minimum for useful forecasts.

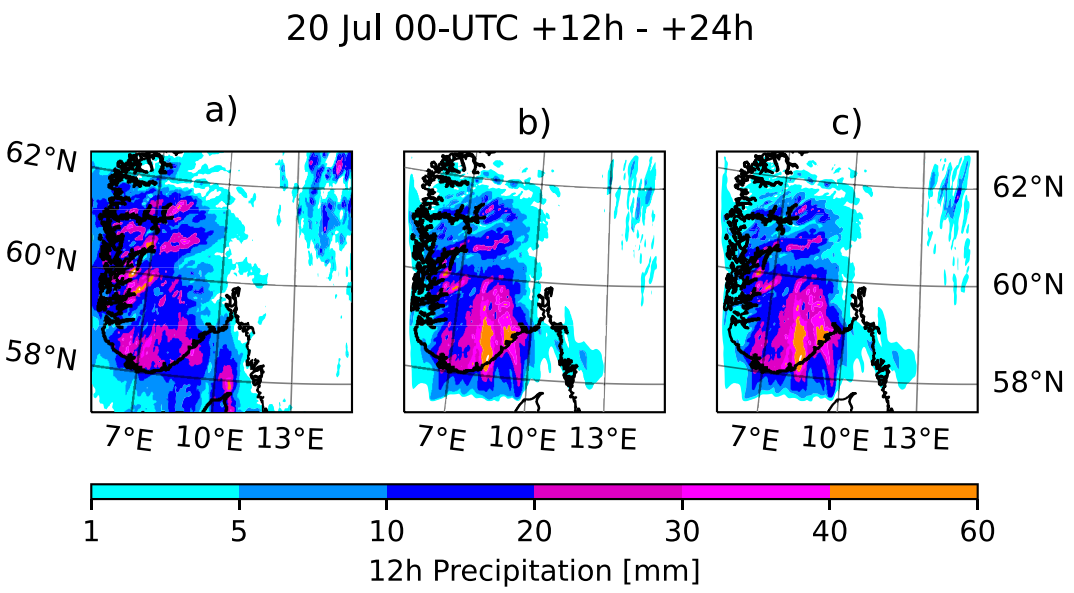

FIG. 11. The 12-h accumulated precipitation from 1200 UTC 20 Jul 2019 to 0000 UTC 21 Jul 2019 for (a) the Nordic Analysis, (b) REF, and (c) OFL.

(i.e., Seneviratne et al. 2010; Orth and Seneviratne 2012); however, they focus on the seasonal to climatic time scale. Further, SM observations have been used to obtain precipitation estimates (Crow et al. 2011; Brocca et al. 2016; Parker and Patrignani 2021). Our study indicates that the SM can be corrected by using knowledge of the fallen precipitation, and that the modified fields have impact on short range forecasts over Scandinavia.

The model minus observation statistics for 2-m temperature and humidity, indicate improved forecasts skill throughout the 48-h prognosis for the experiment initialized from offline surface model runs forced by the Nordic Analysis product (Fig. 6). de Rosnay et al. (2014) showed reduced mean errors when using the EKF relative to the OI scheme. However, no signal was found over Scandinavia. Further, Draper and Reichle (2019) found a reduction in 2-m temperature RMSE of up to 0.4 K and 0.5 g kg^{-1} for specific humidity in certain regions, but over Scandinavia no change was found. The reduction of errors in the latter study are comparable with the one found for temperature in the present study; however, we found a larger reduction in errors of specific humidity at the analysis time of 15 g kg^{-1}. In addition to utilizing additional data sources, such as radar-based precipitation and citizen observations, the OFL system also benefits from using observations hourly during the 3-h assimilation period. In contrast, the REF system only uses observations that are valid at a single point in time and is corrected every 3 h. Consequently, if the model missed precipitation within the 3-h window and the land–atmosphere interactions are weak during this period, the 2-m temperature and humidity will not contain information about the SM and the sequential DA scheme will most likely fail to correct the model state. The land–atmosphere interactions can, however, increase during the following forecast and as a result miscalculate surface fluxes. In this situation, the OFL system will have more realistic SM values and thus give better input for the flux calculation.

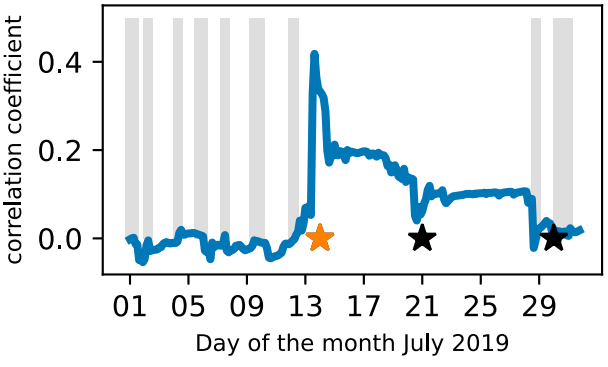

FIG. 12. Correlation coefficient over the domain between 18-h accumulated precipitation differences (Nordic Analysis − REF) on 13 Jul 2019 (orange star) vs SM difference (OFL − REF) per analysis time of July 2019. Markers indicate the three major precipitation events. Gray bars indicate statistically insignificant correlation coefficients at the 95% confidence level.

There is a diurnal variation of temperature errors with smallest errors during the morning and largest errors in the afternoon. The reduction of RMSE in OFL relative to REF is also largest during morning hours. This coincides with the diurnal variation of the soil temperature differences in the model comparison (Fig. 5). Liu and Pu (2019) found that SM has a larger impact on 2-m temperature during daytime. In light of their findings, our results suggest that the ST is the main contributor in improving 2-m temperature during the night. Further, surface moisture and heat fluxes are increased during daytime due to the solar radiation. The increased errors in the afternoon thus indicate that the surface fluxes are inaccurate and introduce errors to the 2-m parameters. Because SM has larger impact on 2-m temperature during

day, one could argue that the SM fields are less certain than the ST and thus lead to larger errors in screen level variables. However, the reduction of forecast errors indicates that more realistic SM estimates are obtained in OFL compared to REF. And, because of the larger magnitude of the surface fluxes during daytime, the parameterization of these becomes important.

There is also a weather-dependent variation of the forecast errors. The standard deviation of 2-m temperature errors decreases during a period with rain and clouds, see Fig. 7. During this period (15–22 July) the two experiments have largest differences in SM and the ST difference has strong diurnal amplitude (Fig. 5). The increase in standard errors of 2-m temperature in the following dry period is likely caused by the strengthened radiative heating during daytime, and thus a larger amplitude of the diurnal variation. OFL has less growth of errors when the standard errors are large, which also coincide with the increasing differences between the models. For the latter period, a reduction in mean errors is also seen in OFL relative to REF. Similar dependency on weather systems were also found by Barthlott and Kalthoff (2011); Keil et al. (2019) when they investigated land–atmosphere interactions and SM–precipitation relationship over central Europe. FSS for precipitation relative to the Nordic Analysis product reveals that the experiment initialized from offline simulations give better spatial accuracy in the convective precipitation case than the reference experiment for higher thresholds. For the other precipitation events driven by large-scale systems, the simulations have indistinguishable FSS. This demonstrates that the dependency of weather regimes on land–atmosphere interaction also applies over this region. Enhanced FSS was also found by Koukoula et al. (2019) in their experiments covering the CONUS with a similar initialization approach. They also found the improved FSS only in the warm season when precipitation was mainly convectively driven. Finally, we emphasize that only one convective event is covered by our experiments and that this is not sufficient to prove a general improvement of precipitation forecasts. However, we have shown that the forecast model is sensitive to surface initial conditions in a physically consistent way, demonstrated through the coupling between surface state, heat fluxes, and subsequently 2-m variable scores. This strengthens our confidence that the improved spatial patterns of the convective precipitation are obtained for the right reasons.

5. Conclusions

Through the experiments performed in this study, we have shown that regional short range NWP forecasts are sensitive, in terms of near surface parameters and the spatial pattern of convective precipitation, to land surface initial conditions. The two different initialization methods produced relatively large differences in soil state throughout the experiment duration, with consecutive modification to the model forecast. The dependency of the ambient weather system on the land–atmosphere coupling strength found in previous publications, is confirmed to be valid also over southern Norway. In global experiments, Scandinavia is usually found to have weak land–atmosphere coupling strength. However, we have shown that in a high-resolution limited-area model, the land surface conditions do impact precipitation patterns in the case of weak synoptic forcing. It is worth commenting that the model domain used in this study can be considered small for the purpose of NWP. One impact of a small domain is that the lateral atmospheric boundaries control the interior weather to a larger degree. We thus argue that the initialization method can have a larger impact if the domain size is increased.

By forcing the LSM with analyzed atmospheric input data, we improved the forecasts of screen level parameters compared to the SEKF scheme. Followingly, it is likely that the analyses of soil variables are also improved; however, the in situ observation network to evaluate this does not exist within the domain, and the available satellite products are not of satisfactory quality. Two main aspects benefiting the alternative method are likely to account for this. First, the alternative method uses a larger amount of observation types, in particular precipitation data from the radar network. It also incorporates observations throughout the cycling period, which is more in line with a continuous DA method like the 4D-Var scheme. We have shown that differences in precipitation forcing can sustain in terms of SM differences for several weeks. The alternative initialization method thus has an advantage over the sequential DA method. Last, by ingesting observations through the atmospheric forcing to the LSM, we avoid the assumptions and simplifications required by the SEKF scheme. In this way, the full nonlinear physics processes the additional information.

In the present study, we have replaced a sequential data assimilation system with an offline cycling of the land surface. However, the method presented here is not capable of utilizing satellite observations of surface variables that are found to improve the estimates of soil variables (Draper et al. 2012; Seo et al. 2021). Therefore, we propose that the method investigated herein should not replace, but supplement an LDA system. In fact, the improved first guess provided with this method can aid the assimilation of surface sensitive satellite channels (English 2008).

Last, this study was focused on the summer season and the impact on convective precipitation. However, Køltzow et al. (2021) found elevated values of potential change in forecast quality over inland areas in northern Scandinavia during the cold season due to large impact of surface data assimilation. Further, Birman et al. (2017) improved the snow depth estimates by assimilating radar precipitation and rain gauge measurements over the French Alps. The adjusted precipitation forcing obtained in our study can also have a large impact on snow accumulation during winter, and evaluation of the alternative initialization method during the cold season is suggested as a future study.

Acknowledgments. The present study is funded and by the Norwegian Meteorological Institute (Met Norway) and is part of the Hydrometeorology to Operations (H2O) project. We thank Morten Køltzow (Met Norway) for fruitful discussions and advice concerning the validation analysis. Finally, we acknowledge the discussions within the Consortium for Convection-scale

Modelling Research and Development (ACCORD) surface community about the concept.

Data availability statement. The Nordic Analysis products are open accessible from the Norwegian Meteorological Institutes thredds server (https://thredds.met.no/thredds/catalog/metpparchivev2/catalog.html) and the in situ observations are accessible through the frost API (https://frost.met.no/).

REFERENCES

Albergel, C., and Coauthors, 2017: Sequential assimilation of satellite-derived vegetation and soil moisture products using SURFEX_v8.0: LDAS-Monde assessment over the Euro-Mediterranean area. *Geosci. Model Dev.*, **10**, 3889–3912, https://doi.org/10.5194/gmd-10-3889-2017.

Balsamo, G., A. Beljaars, K. Scipal, P. Viterbo, B. van den Hurk, M. Hirschi, and A. K. Betts, 2009: A revised hydrology for the ECMWF model: Verification from field site to terrestrial water storage and impact in the integrated forecast system. *J. Hydrometeor.*, **10**, 623–643, https://doi.org/10.1175/2008JHM1068.1.

Barthlott, C., and N. Kalthoff, 2011: A numerical sensitivity study on the impact of soil moisture on convection-related parameters and convective precipitation over complex terrain. *J. Atmos. Sci.*, **68**, 2971–2987, https://doi.org/10.1175/JAS-D-11-027.1.

Båserud, L., C. Lussana, T. N. Nipen, I. A. Seierstad, L. Oram, and T. Aspelien, 2020: TITAN automatic spatial quality control of meteorological in-situ observations. *Adv. Sci. Res.*, **17**, 153–163, https://doi.org/10.5194/asr-17-153-2020.

Baur, F., C. Keil, and G. C. Craig, 2018: Soil moisture–precipitation coupling over central Europe: Interactions between surface anomalies at different scales and the dynamical implication. *Quart. J. Roy. Meteor. Soc.*, **144**, 2863–2875, https://doi.org/10.1002/qj.3415.

Best, M. J., and Coauthors, 2011: The joint UK land environment simulator (JULES), model description—Part 1: Energy and water fluxes. *Geosci. Model Dev.*, **4**, 677–699, https://doi.org/10.5194/gmd-4-677-2011.

Birman, C., F. Karbou, J.-F. Mahfouf, M. Lafaysse, Y. Durand, G. Giraud, L. Mérindol, and L. Hermozo, 2017: Precipitation analysis over the French Alps using a variational approach and study of potential added value of ground-based radar observations. *J. Hydrometeor.*, **18**, 1425–1451, https://doi.org/10.1175/JHM-D-16-0144.1.

Blyverket, J., P. D. Hamer, L. Bertino, C. Albergel, D. Fairbairn, and W. A. Lahoz, 2019: An evaluation of the EnKF vs. EnOI and the assimilation of SMAP, SMOS and ESA CCI soil moisture data over the contiguous U.S. *Remote Sens.*, **11**, 478, https://doi.org/10.3390/rs11050478.

Boone, A., P. Samuelsson, S. Gollvik, A. Napoly, L. Jarlan, E. Brun, and B. Decharme, 2017: The interactions between soil–biosphere–atmosphere land surface model with a multi-energy balance (ISBA-MEB) option in SURFEXv8—Part 1: Model description. *Geosci. Model Dev.*, **10**, 843–872, https://doi.org/10.5194/gmd-10-843-2017.

Brocca, L., and Coauthors, 2016: Rainfall estimation by inverting SMOS soil moisture estimates: A comparison of different methods over Australia. *J. Geophys. Res. Atmos.*, **121**, 12 062–12 079, https://doi.org/10.1002/2016JD025382.

Calvet, J.-C., J. Noilhan, J.-L. Roujean, P. Bessemoulin, M. Cabelguenne, A. Olioso, and J.-P. Wigneron, 1998: An interactive vegetation SVAT model tested against data from six contrasting sites. *Agric. For. Meteor.*, **92**, 73–95, https://doi.org/10.1016/S0168-1923(98)00091-4.

Cioni, G., and C. Hohenegger, 2017: Effect of soil moisture on diurnal convection and precipitation in large-eddy simulations. *J. Hydrometeor.*, **18**, 1885–1903, https://doi.org/10.1175/JHM-D-16-0241.1.

Crow, W. T., M. J. van den Berg, G. J. Huffman, and T. Pellarin, 2011: Correcting rainfall using satellite-based surface soil moisture retrievals: The soil moisture analysis rainfall tool (SMART). *Water Resour. Res.*, **47**, W08521, https://doi.org/10.1029/2011WR010576.

Danielson, J. J., and D. B. Gesch, 2011: Global multi-resolution terrain elevation data 2010 (GMTED2010). Tech. Rep. 2011-1073, 29 pp., https://doi.org/10.3133/ofr20111073.

Decharme, B., A. Boone, C. Delire, and J. Noilhan, 2011: Local evaluation of the Interaction between Soil Biosphere Atmosphere soil multilayer diffusion scheme using four pedotransfer functions. *J. Geophys. Res.*, **116**, D20126, https://doi.org/10.1029/2011JD016002.

de Rosnay, P., G. Balsamo, C. Albergel, J. Muñoz-Sabater, and L. Isaksen, 2014: Initialisation of land surface variables for numerical weather prediction. *Surv. Geophys.*, **35**, 607–621, https://doi.org/10.1007/s10712-012-9207-x.

Draper, C. S., and R. H. Reichle, 2019: Assimilation of satellite soil moisture for improved atmospheric reanalyses. *Mon. Wea. Rev.*, **147**, 2163–2188, https://doi.org/10.1175/MWR-D-18-0393.1.

——, J.-F. Mahfouf, and J. P. Walker, 2009: An EKF assimilation of AMSR-E soil moisture into the ISBA land surface scheme. *J. Geophys. Res.*, **114**, D20104, https://doi.org/10.1029/2008JD011650.

——, R. H. Reichle, G. J. M. De Lannoy, and Q. Liu, 2012: Assimilation of passive and active microwave soil moisture retrievals. *Geophys. Res. Lett.*, **39**, L04401, https://doi.org/10.1029/2011GL050655.

English, S. J., 2008: The importance of accurate skin temperature in assimilating radiances from satellite sounding instruments. *IEEE Trans. Geosci. Remote Sens.*, **46**, 403–408, https://doi.org/10.1109/TGRS.2007.902413.

Fairbairn, D., P. de Rosnay, and P. A. Browne, 2019: The new stand-alone surface analysis at ECMWF: Implications for land–atmosphere DA coupling. *J. Hydrometeor.*, **20**, 2023–2042, https://doi.org/10.1175/JHM-D-19-0074.1.

Faroux, S., A. T. Kaptué Tchuenté, J.-L. Roujean, V. Masson, E. Martin, and P. Le Moigne, 2013: ECOCLIMAP-II/Europe: A twofold database of ecosystems and surface parameters at 1 km resolution based on satellite information for use in land surface, meteorological and climate models. *Geosci. Model Dev.*, **6**, 563–582, https://doi.org/10.5194/gmd-6-563-2013.

Findell, K. L., and E. A. B. Eltahir, 2003: Atmospheric controls on soil moisture–boundary layer interactions. Part I: Framework development. *J. Hydrometeor.*, **4**, 552–569, https://doi.org/10.1175/1525-7541(2003)004<0552:ACOSML>2.0.CO;2.

Fisher, R. A., and C. D. Koven, 2020: Perspectives on the future of land surface models and the challenges of representing complex terrestrial systems. *J. Adv. Model. Earth Syst.*, **12**, e2018MS001453, https://doi.org/10.1029/2018MS001453.

Ghent, D., J. Kaduk, J. Remedios, J. Ardö, and H. Balzter, 2010: Assimilation of land surface temperature into the land surface model JULES with an ensemble Kalman filter. *J. Geophys. Res.*, **115**, D19112, https://doi.org/10.1029/2010JD014392.

Gómez, B., C. L. Charlton-Pérez, H. Lewis, and B. Candy, 2020: The Met Office operational soil moisture analysis system. *Remote Sens.*, **12**, 3691, https://doi.org/10.3390/rs12223691.

Grinde, L., J. Mamen, and K. Tunheim, 2019: Været i Norge (Weather in Norway). Met-info. Tech. Rep., Meteorologisk Institutt,19 pp., https://www.met.no/publikasjoner/met-info/met-info-2019/_/attachment/download/0d9d8654-3afa-42e1-87aa-a66be76d9278:416ffdf68a3486eea88acb70145c85abe0d4093c/MET-info-07-2019.pdf.

Hengl, T., and Coauthors, 2017: SoilGrids250m: Global gridded soil information based on machine learning. *PLOS ONE*, **12**, e0169748, https://doi.org/10.1371/journal.pone.0169748.

Henneberg, O., F. Ament, and V. Grützun, 2018: Assessing the uncertainty of soil moisture impacts on convective precipitation using a new ensemble approach. *Atmos. Chem. Phys.*, **18**, 6413–6425, https://doi.org/10.5194/acp-18-6413-2018.

Keil, C., F. Baur, K. Bachmann, S. Rasp, L. Schneider, and C. Barthlott, 2019: Relative contribution of soil moisture, boundary-layer and microphysical perturbations on convective predictability in different weather regimes. *Quart. J. Roy. Meteor. Soc.*, **145**, 3102–3115, https://doi.org/10.1002/qj.3607.

Køltzow, M., R. Grote, and A. Singleton, 2021: On the configuration of a regional Arctic numerical weather prediction system to maximize predictive capacity. *Tellus*, **73A**, 1976093, https://doi.org/10.1080/16000870.2021.1976093.

Koster, R. D., and Coauthors, 2006: GLACE: The Global Land–Atmosphere Coupling Experiment. Part I: Overview. *J. Hydrometeor.*, **7**, 590–610, https://doi.org/10.1175/JHM510.1.

Koukoula, M., E. I. Nikolopoulos, J. Kushta, N. S. Bartsotas, G. Kallos, and E. N. Anagnostou, 2019: A numerical sensitivity analysis of soil moisture feedback on convective precipitation. *J. Hydrometeor.*, **20**, 23–44, https://doi.org/10.1175/JHM-D-18-0134.1.

——, C. S. Schwartz, E. I. Nikolopoulos, and E. N. Anagnostou, 2021: Understanding the impact of soil moisture on precipitation under different climate and meteorological conditions: A numerical sensitivity study over the CONUS. *J. Geophys. Res. Atmos.*, **126**, e2021JD035096, https://doi.org/10.1029/2021JD035096.

Lawrence, D. M., and Coauthors, 2019: The Community Land Model version 5: Description of new features, benchmarking, and impact of forcing uncertainty. *J. Adv. Model. Earth Syst.*, **11**, 4245–4287, https://doi.org/10.1029/2018MS001583.

Liu, J., and Z. Pu, 2019: Does soil moisture have an influence on near-surface temperature? *J. Geophys. Res. Atmos.*, **124**, 6444–6466, https://doi.org/10.1029/2018JD029750.

Lussana, C., I. A. Seierstad, T. N. Nipen, and L. Cantarello, 2019: Spatial interpolation of two-metre temperature over Norway based on the combination of numerical weather prediction ensembles and *in situ* observations. *Quart. J. Roy. Meteor. Soc.*, **145**, 3626–3643, https://doi.org/10.1002/qj.3646.

——, T. N. Nipen, I. A. Seierstad, and C. A. Elo, 2021: Ensemble-based statistical interpolation with Gaussian anamorphosis for the spatial analysis of precipitation. *Nonlinear Processes Geophys.*, **28**, 61–91, https://doi.org/10.5194/npg-28-61-2021.

Maggioni, V., E. N. Anagnostou, and R. H. Reichle, 2012: The impact of model and rainfall forcing errors on characterizing soil moisture uncertainty in land surface modeling. *Hydrol. Earth Syst. Sci.*, **16**, 3499–3515, https://doi.org/10.5194/hess-16-3499-2012.

Mahfouf, J.-F., 1991: Analysis of soil moisture from near-surface parameters: A feasibility study. *J. Appl. Meteor.*, **30**, 1534–1547, https://doi.org/10.1175/1520-0450(1991)030<1534:AOSMFN>2.0.CO;2.

——, K. Bergaoui, C. Draper, F. Bouyssel, F. Taillefer, and L. Taseva, 2009: A comparison of two off-line soil analysis schemes for assimilation of screen level observations. *J. Geophys. Res.*, **114**, D08105, https://doi.org/10.1029/2008JD011077.

Masson, V., J.-L. Champeaux, F. Chauvin, C. Meriguet, and R. Lacaze, 2003: A global database of land surface parameters at 1-km resolution in meteorological and climate models. *J. Climate*, **16**, 1261–1282, https://doi.org/10.1175/1520-0442(2003)16%3C1261:AGDOLS%3E2.0.CO;2.

——, and Coauthors, 2013: The SURFEXv7.2 land and ocean surface platform for coupled or offline simulation of Earth surface variables and fluxes. *Geosci. Model Dev.*, **6**, 929–960, https://doi.org/10.5194/gmd-6-929-2013.

Müller, M., and Coauthors, 2017: AROME-MetCoOp: A Nordic convective-scale operational weather prediction model. *Wea. Forecasting*, **32**, 609–627, https://doi.org/10.1175/WAF-D-16-0099.1.

Napoly, A., and Coauthors, 2017: The Interactions between Soil–Biosphere–Atmosphere (ISBA) land surface model multi-energy balance (MEB) option in SURFEXv8—Part 2: Introduction of a litter formulation and model evaluation for local-scale forest sites. *Geosci. Model Dev.*, **10**, 1621–1644, https://doi.org/10.5194/gmd-10-1621-2017.

Nipen, T. N., I. A. Seierstad, C. Lussana, J. Kristiansen, and Ø. Hov, 2020: Adopting citizen observations in operational weather prediction. *Bull. Amer. Meteor. Soc.*, **101**, E43–E57, https://doi.org/10.1175/BAMS-D-18-0237.1.

Noilhan, J., and J.-F. Mahfouf, 1996: The ISBA land surface parameterisation scheme. *Global Planet. Change*, **13**, 145–159, https://doi.org/10.1016/0921-8181(95)00043-7.

Orth, R., and S. I. Seneviratne, 2012: Analysis of soil moisture memory from observations in Europe. *J. Geophys. Res.*, **117**, D15115, https://doi.org/10.1029/2011JD017366.

Parker, N., and A. Patrignani, 2021: Reconstructing precipitation events using collocated soil moisture information. *J. Hydrometeor.*, **22**, 3275–3290, https://doi.org/10.1175/JHM-D-21-0168.1.

Reichle, R. H., D. B. McLaughlin, and D. Entekhabi, 2002: Hydrologic data assimilation with the ensemble Kalman filter. *Mon. Wea. Rev.*, **130**, 103–114, https://doi.org/10.1175/1520-0493(2002)130<0103:HDAWTE>2.0.CO;2.

——, Q. Liu, R. D. Koster, C. S. Draper, S. P. P. Mahanama, and G. S. Partyka, 2017: Land surface precipitation in MERRA-2. *J. Climate*, **30**, 1643–1664, https://doi.org/10.1175/JCLI-D-16-0570.1.

Roberts, N. M., and H. W. Lean, 2008: Scale-selective verification of rainfall accumulations from high-resolution forecasts of convective events. *Mon. Wea. Rev.*, **136**, 78–97, https://doi.org/10.1175/2007MWR2123.1.

Santanello, J. A., Jr., P. Lawston, S. Kumar, and E. Dennis, 2019: Understanding the impacts of soil moisture initial conditions on NWP in the context of land–atmosphere coupling. *J. Hydrometeor.*, **20**, 793–819, https://doi.org/10.1175/JHM-D-18-0186.1.

Seity, Y., P. Brousseau, S. Malardel, G. Hello, P. Bénard, F. Bouttier, C. Lac, and V. Masson, 2011: The AROME-France convective-scale operational model. *Mon. Wea. Rev.*, **139**, 976–991, https://doi.org/10.1175/2010MWR3425.1.

Seneviratne, S. I., T. Corti, E. L. Davin, M. Hirschi, E. B. Jaeger, I. Lehner, B. Orlowsky, and A. J. Teuling, 2010: Investigating soil moisture–climate interactions in a changing climate: A review. *Earth Sci. Rev.*, **99**, 125–161, https://doi.org/10.1016/j.earscirev.2010.02.004.

——, and Coauthors, 2013: Impact of soil moisture-climate feedbacks on CMIP5 projections: First results from the GLACE-

CMIP5 experiment. *Geophys. Res. Lett.*, **40**, 5212–5217, https://doi.org/10.1002/grl.50956.

Seo, E., M.-I. Lee, and R. H. Reichle, 2021: Assimilation of SMAP and ASCAT soil moisture retrievals into the JULES land surface model using the local ensemble transform Kalman filter. *Remote Sens. Environ.*, **253**, 112222, https://doi.org/10.1016/j.rse.2020.112222.

van den Hurk, B., F. Doblas-Reyes, G. Balsamo, R. D. Koster, S. I. Seneviratne, and H. Camargo Jr., 2012: Soil moisture effects on seasonal temperature and precipitation forecast scores in Europe. *Climate Dyn.*, **38**, 349–362, https://doi.org/10.1007/s00382-010-0956-2.

Wrona, E., T. L. Rowlandson, M. Nambiar, A. A. Berg, A. Colliander, and P. Marsh, 2017: Validation of the soil moisture active passive (SMAP) satellite soil moisture retrieval in an Arctic tundra environment. *Geophys. Res. Lett.*, **44**, 4152–4158, https://doi.org/10.1002/2017GL072946.